


Article

X-ray Induced Hydroxyl Radical Generation by GdYVO₄:Eu³⁺ Nanoparticles in Aqueous Solution: Main Mechanisms

Pavel O. Maksimchuk, Svetlana L. Yefimova, Valeriia V. Omielaieva, Kateryna O. Hubenko, Vladimir K. Klochkov, Oleksandr D. Opolonin and Yuri V. Malyukin * 

Institute for Scintillation Materials National Academy of Sciences of Ukraine, 60 Nauky ave., 61072 Kharkiv, Ukraine; maksimchuk@isma.kharkov.ua (P.O.M.); ephimova@isma.kharkov.ua (S.L.Y.); leravalesya@gmail.com (V.V.O.); gubenko@isma.kharkov.ua (K.O.H.); klochkov@isma.kharkov.ua (V.K.K.); opolonin@isma.kharkov.ua (O.D.O.)

* Correspondence: malyukin.yuri57@gmail.com or malyukin@isma.kharkov.ua

Received: 14 April 2020; Accepted: 2 May 2020; Published: 5 May 2020



Abstract: We report on strong X-ray-induced hydroxyl radical ($\cdot\text{OH}$) generation in an aqueous solution containing UV light pre-treated GdYVO₄:Eu³⁺ nanoparticles (L-GdYVO). The methods of optical spectroscopy were used to detect $\cdot\text{OH}$ in the solutions. The complex nature of the mechanism of $\cdot\text{OH}$ generation has been revealed and discussed. The experimental data obtained indicate that the mechanism of $\cdot\text{OH}$ generation is associated with two main processes: (i) direct $\cdot\text{OH}$ generation with the participation of thermalized h^+ formed at X-ray irradiation, and (ii) X-ray-facilitated jumps of h^+ formed in the nanoparticles' (NPs') valence band at UV light pre-treatment and trapped in local levels formed by random scattering potential. At the same time, for GdYVO₄:Eu³⁺ nanoparticles, which were not exposed to UV light before the X-ray irradiation (D-GdYVO), a strong radioprotective effect ascribed to the electron-donation properties of V⁴⁺ ions was observed. Thus, depending on the pre-treatment condition, we can change the redox properties of GdYVO₄:Eu³⁺ NPs in an opposite direction, which makes this nanomaterial a unique theranostic agent for radiation therapy (RT) enhancement, allowing the problem of radiation therapy (RT)-resistant hypoxic tumours to be overcome.

Keywords: nanocrystals; X-ray irradiation; hydroxyl radical generation; radioprotective effect

1. Introduction

Radiation therapy (RT), i.e., the use of ionizing radiation for cancer treatment, has become one of the first-line treatment modalities in oncology [1–4]. An estimated 60% of all cancer patients receive RT during their course of illness, either alone or in combination with chemotherapy or surgery [3,4]. X-rays or γ -rays used for RT can destroy cancer cells either by directly damaging the nuclear material (DNA) or by ionization/excitation of the water component of the cells. In the latter case, water is sequentially converted into a number of radicals and molecular products: hydrated electrons (e_{aq}^-), hydrogen atoms ($\text{H}\cdot$), hydroxyl radicals ($\cdot\text{OH}$), hydroperoxyl radicals ($\text{HO}_2\cdot$), hydrogen peroxide (H_2O_2), and hydrogen molecules (H_2) [5–8]. In addition, hydrated electrons are known to be strong reducing agents and can reduce O_2 dissolved in water to a highly reactive superoxide anion (O_2^-). However, despite the great advances of RT, many challenges remain. One of them is normal tissue toxicity. As photons interact not only with tumour tissues, severe side effects or even secondary cancers may be induced when healthy tissues are damaged [7,9]. The second challenge is innate or acquired radioresistance in a number of cancers (e.g., hypoxic tumours such as pancreatic cancer and glioblastoma) [9–11]. Solid tumours are

known to be very heterogeneous and composed of different areas: regions saturated with oxygen and oxygen-deficient, hypoxic ones. The hypoxic regions possess some resistance to radiotherapy due to the lack of molecular oxygen required to form superoxide anions, one of the highly reactive oxygen species (ROS) [9,10].

Several approaches were proposed to overcome these challenges, including fractionating the radiation dose over time or over space, and the systemic administration of protective drugs to neutralize the effect of free radicals in healthy cells [1,2,12]. Recently, a promising strategy based on the application of nanoparticles (NPs) has been proposed to increase of RT efficiency [4,9,11–13]. The preferential accumulation of NPs in the tumour due to the enhanced permeability and retention (EPR) effect can offer a solution for many challenges by (i) improving contrast enhancement for image-guided RT; (ii) ensuring tumour-specific delivery of chemotherapeutic agents for combined chemo-RT, and (iii) increasing the local dose of radiation using particles with high atomic numbers (Z) [7,14]. The absorption of X-ray photons by high Z atom elements results mainly in the inner-shell electron ejection (photoelectric effect) and Compton electron scattering. For keV energy photons (typically < 100 keV), photoelectric absorption is the dominant interaction process [11–17]. Photoelectric cross-section is known to be strongly dependent on Z as $\sigma_{pe} \propto Z^n/E^3$, where E is the energy of the incoming photon and Z is the atomic number of the atom being targeted, and n varies between 4 and 5 depending on the E value. Photoelectrons, Auger electrons, and secondary electrons formed at X-ray irradiation may successively ionize surrounding biomolecules and hydrolyse water molecules within the cells that induce more effective DNA damage in a nanoparticle-loaded biosystem [12–16].

Among various high-Z nanomaterials investigated for RT enhancement, so called nano-radio-enhancers (NRE), NPs on the base of gold [8,14,18], platinum [14], hafnium [13], and gadolinium [18–21], are the most studied. All of these NRE were shown to increase the radiation dose and RT efficiency both in vitro and in vivo due to the high Z-effect and a number of specific properties. However, it should be noted that despite the above-mentioned advantages, NREs are still in the very early translational stages, with nearly all efforts devoted to preclinical studies due to some significant drawbacks including long blood half-life, accumulation in the liver, spleen, and other tissue, poor whole-body clearance, and skin coloration (Au and Ag NPs) [7,22]. Among these NPs, gadolinium-based ones can be regarded as a prospective theranostic agent, which could ensure both increasing RT efficiency and the monitoring of the radiosensitizing agent within the tumour due to paramagnetic features of gadolinium ions used for enhancing magnetic resonance imaging contrast [19–21]. For Gd-based NPs called AGuIX[®], low toxicity in animals and the possibility of intravenous administration were reported, allowing them to be used in Phase I clinical trials in humans with brain metastasis [19]. Our recent studies revealed the changeable pro-/anti-oxidant action of small 2 nm gadolinium–yttrium orthovanadate NPs doped with Eu³⁺ ions (GdYVO₄:Eu³⁺), i.e., the ability of O₂^{•−} and ·OH generation or scavenging depending on external conditions [23]. In an in vivo experiment, protective properties against X-ray-induced damage of GdVO₄:Eu³⁺ NPs were reported [24].

Moreover, effective dark ·OH generation by water splitting via the hole-mediated reaction was also detected [25], which shows the potential of GdYVO₄:Eu³⁺ NPs for RT treatment of aggressive hypoxic tumours as for ·OH generation, the presence of molecular oxygen is not required.

In modern RT applications, high-energy beams of 2–25 MeV (“deep” X-ray) are commonly used, which allows deep tumours (>2 cm in depth) to be reached [11,16,26]. However, it should be noted that low-energy beams in the range of 40–100 keV (“superficial” X-rays) are used for skin cancer or the treatment of other exposed structures (e.g., melanoma, basal cell carcinoma, squamous cell carcinoma, keloid) [11,16,25]. Low-energy X-ray beams are reported to be used in RT/photodynamic “hybrid” therapy using scintillation NPs and also in image-guided RT applications [16,26]. Gd₂O₃, Bi₂O₃, Au, and Fe-based NPs and a variety of scintillation NPs containing lanthanide ions excited with the low-energy X-ray beams were used in these applications (see reviews [16,26]).

This paper extends our work on GdYVO₄:Eu³⁺ NPs redox activity studies [23–25]. The effects of X-ray irradiation and pre-treatment conditions on GdYVO₄:Eu³⁺ NP redox properties in aqueous solutions were studied.

2. Materials and Methods

2.1. Synthesis of GdYVO₄:Eu³⁺ NPs and Their Characterization

Gadolinium–yttrium orthovanadate NPs doped with europium ions GdYVO₄:Eu³⁺ (GdYVO) were synthesized by the method reported in our previous paper [24,27]. First, 10 mL of aqueous solution of 0.01 M lanthanide chlorides (99.9% Acros Organics, Geel, Belgium) was prepared by mixing 7 mL of GdCl₃, 2 mL of YCl₃, and 1 mL of EuCl₃. Then 8 mL of 0.01 M sodium citrate solution (99%, Acros Organics, Geel, Belgium) was added, and then 8 mL 0.01 M Na₃VO₄ was flowed drop-wise (pH = 13) to the obtained mixture. The mixture was intensively stirred using a magnetic stirrer to obtain a transparent solution and then heated in a water bath for 30 min at 100 °C. Then the solution was cooled, and the excess of ions was removed by dialysis against water for 24 h. The obtained aqueous colloidal solution containing GdYVO NPs was characterized by transmission electron microscopy (TEM), Fourier-transform infrared spectroscopy (FT-IR), X-ray powder diffraction analysis (XRD), dynamic light scattering (DLS) analysis, and UV-vis optical spectroscopy.

To obtain TEM images of synthesized GdYVO, a TEM-125K electron microscope with a 100 kV electron beam (Selmi, Ukraine) was used. For sample preparation, 200 mesh carbon-coated Cu grids (Electron Microscopy Sciences, Hatfield, PA, USA) were used. A 5 µL drop of the colloidal solution was deposited to a grid and the solvent allowed to evaporate.

A FT-IR spectrum was obtained on a Perkin-Elmer Spectrum One B FT-IR spectrometer (PerkinElmer, Inc., Waltham, MA, USA) in the range of 4000–400 cm⁻¹ using KBr pellets. To obtain GdYVO powder, the colloidal solution was dried at 80 °C.

An X-ray diffraction pattern of GdYVO was obtained with a Siemens D500 X-ray diffractometer (Siemens, Berlin, Germany).

Hydrodynamic diameter and ζ-potentials of synthesized GdYVO NPs were measured using a ZetaPALS/BI-MAS analyser (Brookhaven Instruments Corp., Holtsville, NY, USA) operated in the phase analysis light-scattering mode.

UV-vis absorption spectra were obtained using a Specord 200 UV-vis spectrometer (Analytik Jena, Jena, Germany).

2.2. Measurement of ·OH Generation in Aqueous Solutions under X-Ray Irradiation

For the detection of ·OH generation in the solutions with/without GdYVO NPs, an ·OH-specific probe 1,2-Benzopyrone (coumarin, Sigma-Aldrich) was used [28]. The route of OH detection is based on the formation in a solution of fluorescent product of the coumarin oxidation (7-hydroxycoumarin), which could be registered by the appearance of a new fluorescent band with a maximum at 460 nm. First, a stock solution of coumarin (0.1 mmol L⁻¹) in bi-distilled water was prepared. Then necessary amount of the coumarin stock solution was mixed with the colloidal GdYVO NP solutions (dark-stored or UV light pre-irradiated) to reach final coumarin and NP concentrations of 0.1 mmol L⁻¹ and 1 g L⁻¹, respectively. The obtained solutions containing GdYVO NPs and coumarin were placed in plastic cuvettes (10 × 10 mm) and irradiated from the open part by X-ray radiation using an ISOVOLT 160 Titan E device with a tungsten anode for different time intervals (10, 20, or 30 min). The voltage on the tube was 30 kV (20 mA). The distance from the X-ray tube to the irradiated samples was 25 cm. The absorbed dose rate in air of 0.0143 Gy/min was estimated using the free software Rad Pro Calculator Version 3.26, taking an irradiated field of 1 × 1 cm². The absorbed doses are 0.14, 0.28, and 0.42 Gy for 10, 20, and 30 min of X-ray irradiation, respectively.

Then the solutions were poured into quartz cuvettes, and fluorescence intensities (exc/em 325/460 nm) were measured on a Lumina spectrofluorimeter (Thermo Scientific, Madison, WI, USA). To estimate $\cdot\text{OH}$ generation, the relative intensity of the maxima centred at 460 nm was analysed.

3. Results and Discussion

The as-synthesized GdYVO exhibits spherical-like particles with about a 2 nm diameter (Figure 1a). Their crystalline phase was determined using XRD to be a tetrahedral zircon-type structure of GdVO₄ (JCPDS, no. 72-0277, Figure 1b). The FT-IR spectrum of the GdYVO powder confirms the crystal structure of synthesized NPs, revealing a strong absorption peak at 792 cm⁻¹ and a weaker one at 445 cm⁻¹, which correspond to stretching vibrations of V–O and Re(Eu)–O bands, respectively (Figure 1c) [29,30]. The broad band at the range of 2900–3700 cm⁻¹ belongs to the water O–H stretching vibrations. Note that for GdYVO NP stabilization in aqueous solution, the synthesis routine includes the addition of a stabilizer, sodium citrate. Peaks at 1391 cm⁻¹ and 1570 cm⁻¹ in the FT-IR spectrum are associated with symmetrical and asymmetrical vibrations of carboxylate groups of the stabilizer. The weak peaks at 1072 and 1259 cm⁻¹ belong to vibrations of the C–O citrate bond, whereas ones at 2928 cm⁻¹ and 2865 cm⁻¹ are associated with the vibrations of CH groups of the carboxylate group shells at the surface of GdYVO [31,32].

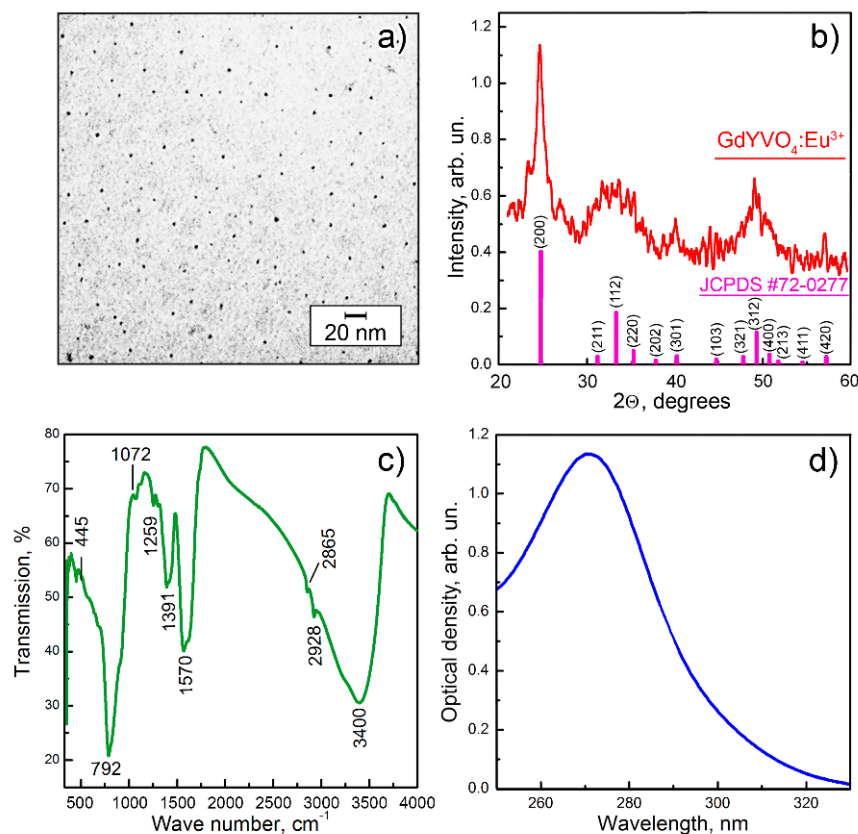


Figure 1. TEM image (a), XRD pattern (b), FT-IR spectrum (c), and absorption spectrum (d) of synthesized GdYVO.

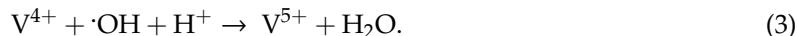
Negatively charged carboxylate groups of a citrate ion stabilizer impart a negative charge to the surface of GdYVO NPs (ζ -potential is -20.94 ± 1.27 mV) and, consequently, high stability of the synthesized colloidal solution. The hydrodynamic diameter (d_h) of GdYVO is determined to be 25 ± 1.3 nm. The higher value of NP size as compared with the data obtained with TEM microscopy is due to hydrate and stabilizer ion shells at the surface of NPs.

Figure 1d represents the absorption spectrum of GdYVO, with a characteristic asymmetric broad band within the 250–350 nm spectral range associated with a charge transfer from oxygen to the vanadium ions in VO_4^{3-} groups of the GdYVO crystal lattice [33,34]. GdYVO belongs to the direct gap semiconductors family; the band gap energy (E_g) was estimated to be 4.25 eV using Tauc's relationship [23]. That means that at high energy excitation ($E > E_g$), in GdYVO a charge separation could be created with a generation of e^- in the conduction band (CB) and h^+ in the valence band (VB), which could participate in a variety of redox reactions with a formation of ROS, mainly $\cdot OH$ generation by the h^+ -mediated H_2O splitting reaction and O_2^- production via the e^- -mediated O_2 reduction [23,25].



The VB of vanadate nanocrystals was found to be mainly composed of oxygen 2p orbitals [35]. Small $ReVO_4$ NPs were reported to possess a large amount of oxygen vacancies V_O and conjunct V^{4+} ions [36–38]. A large amount of such V_O forms random scattering potentials (RSPs), which could serve as h^+ traps above the top of VB and hinder h^+ jump movement to the surface of NPs [23,25,39] and consequent participation in the water splitting reaction (2). Recently, we have reported that h^+ formed at NP UV light irradiation and trapped on such localized levels can be stored up to 4 days and is responsible for dark $\cdot OH$ generation [24]. Note that $\cdot OH$ generation by UV light pre-treated GdYVO NPs in dark conditions is very effective and comparable to that observed at direct NP UV irradiation [25].

At the same time, in GdYVO NPs a competitive ROS scavenging mechanism occurs and is associated with $V^{4+}-V_O-V^{4+}$ complexes as well [23]. Electrons stored in V^{4+} ions as a result of V_O formation can participate in ROS neutralization, in particular, hydroxyl radicals:



The ROS scavenging mechanism was shown to be dominant in the first stage of GdYVO UV irradiation and then depleted due to V^{4+} oxidation [40].

Based the experimental facts stated above, in our experiments with X-ray irradiation, we use two groups of GdYVO NPs: (i) GdYVO NPs, which were kept in the dark before the experiment in order to deplete h^+ localized levels (marked as D-GdYVO) and (ii) GdYVO NPs, which were UV light pre-treated for 1, 2, or 4 h (marked as L-GdYVO).

Figure 2 plots the mass attenuation coefficient for GdYVO and indicates that at the X-ray irradiation conditions used ($V = 30$ kV), the dominant process in X-ray interaction with the matter is the photoelectric effect; GdYVO contributes to the photoelectric effect by attenuating low-energy X-ray photons. Such an interaction finally gives rise to the generation of e^- and h^+ in CB and VB, respectively.

Figure 3 depicts $\cdot OH$ generation at X-ray irradiation (20 min, 0.28 Gy) in aqueous solutions containing GdYVO NPs. Let us emphasize that according to general principles, at X-ray irradiation of an aqueous solution, the main part of incident high-energy quanta will be absorbed by water, causing its radiolysis with a generation of $\cdot OH$ as a main product [6] (see column 1, Figure 3a,b). However, the addition of GdYVO NPs changes remarkably the patterns of $\cdot OH$ generation in the solution. Moreover, the observed effects depend strongly on NP pre-treatment conditions (columns 2, 3 in Figure 3). In the solution containing D-GdYVO, the amount of $\cdot OH$ detected after 20 min of X-ray irradiation is about 40% smaller than that in pure water solution. Based on our previous data, this effect could be explained by the elimination of $\cdot OH$ (reaction (3)) generated in the solution as a result of both water radiolysis and water splitting on the surface of D-GdYVO NPs via reaction (2). The small size of GdYVO NPs with a high amount of $V^{4+}-V_O-V^{4+}$ and a large surface area for $\cdot OH$ adsorption ensures the high efficiency of this process (Figure 3, column 2). Although an $\cdot OH$ generation process in D-GdYVO at X-ray irradiation is also expected, the ROS scavenging mechanism is dominant.

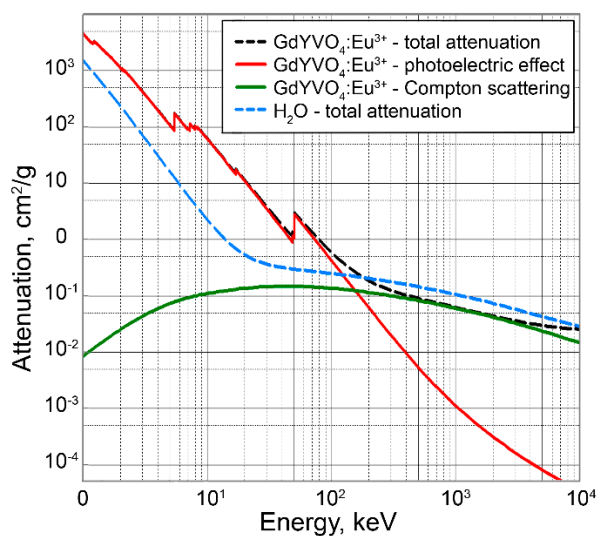


Figure 2. Mass attenuation coefficient as a function of energy for GdYVO.

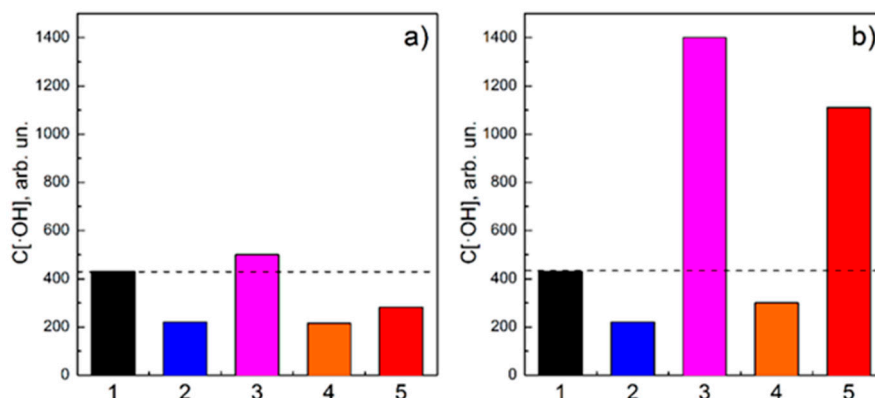


Figure 3. $\cdot\text{OH}$ generation at X-ray irradiation (20 min, 0.28 Gy) of the solutions containing D-GdYVO and L-GdYVO, UV light pre-irradiated for 1 h (a) and 4 h (b): column 1—water solution without NPs (control), column 2—D-GdYVO; column 3—L-GdYVO; 4—L-GdYVO, which did not undergo X-ray irradiation; column 5— $\cdot\text{OH}$ generation in L-GdYVO without the contribution of dark $\cdot\text{OH}$ generation.

At the same time, in the solutions containing L-GdYVO, the amount of $\cdot\text{OH}$ is found to be larger as compared with that in solutions without NPs. Moreover, L-GdYVO UV light pre-irradiation time affects directly the amount of $\cdot\text{OH}$ formed in the solution after 20 min X-ray irradiation (Figure 3a,b column 3). To explain this phenomenon, let us consider the main processes associated with ROS generation or scavenging, which take place during L-GdYVO X-ray irradiation.

(i) Note that in L-GdYVO NPs, the radical scavenging mechanism cannot be dominant or noticeable, because as it was shown earlier [38], UV light irradiation of NPs causes V^{4+} oxidation to V^{5+} via reaction (3).

(ii) Dark $\cdot\text{OH}$ generation (i.e., generation of $\cdot\text{OH}$ with the participation of h^+ stored during UV light pre-irradiation of L-GdYVO) should be also taken into consideration. To address this item, the same portion of L-GdYVO was left on the table without X-ray irradiation, and then the amount of $\cdot\text{OH}$ formed in that solution in the same time interval (20 min) was analysed (Figure 3, column 4).

(iii) X-ray-induced $\cdot\text{OH}$ generation in L-GdYVO via reaction (2). One of the possible ways of excited energy dissipation excepting photoelectrons, Auger electron and secondary electron formation is known to be a thermalization of charge carriers. Electrons are concentrated at the bottom of the CB, whereas holes “float” to the top of the VB and, consequently, are able to participate in ROS production reactions. To separate the X-ray-induced $\cdot\text{OH}$ generation in L-GdYVO, we have subtracted column

4 from column 3 (Figure 3). Thus, column 5 in Figure 3 represents the amount of $\cdot\text{OH}$ generated as a result of L-GdYVO X-ray irradiation without a contribution of dark $\cdot\text{OH}$ generation occurring simultaneously. Figure 3b shows that the time of L-GdYVO UV light pre-treatment sufficiently affects the amount of generated $\cdot\text{OH}$ during the same X-ray irradiation interval. UV light pre-treatment during 4 h gives about a 4 times higher amount of $\cdot\text{OH}$ as compared with that for 1 h of UV light pre-treatment, while the amount of dark-generated $\cdot\text{OH}$ increases not sufficiently (Figure 3a,b, columns 4,5).

Increasing the X-ray irradiation time while keeping constant the time of UV light pre-treatment also enhances the amount of $\cdot\text{OH}$ generated in the solutions containing L-GdYVO (Figure 4, column 3). Moreover, the X-ray-induced $\cdot\text{OH}$ generation is enhanced 3 times with 30 min of X-ray exposure, whereas the amount of dark-generated $\cdot\text{OH}$ increases again not sufficiently (Figure 4, columns 4 and 5, respectively).

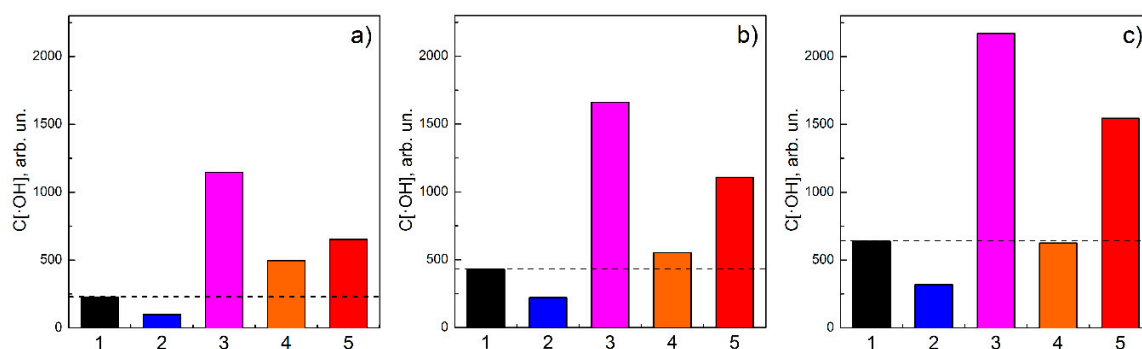


Figure 4. Effect of X-ray exposure time on $\cdot\text{OH}$ generation in the solutions containing D-GdYVO and L-GdYVO UV-light pre-irradiated during 2 h: X-ray exposure 10 min, 0.14 Gy (a), 20 min, 0.28 Gy (b), and 30 min, 0.42 Gy (c). Column 1—water solution without NPs (control), column 2—D-GdYVO; column 3—L-GdYVO; 4—L-GdYVO, which did not undergo X-ray irradiation; column 5— $\cdot\text{OH}$ generation in L-GdYVO without a contribution of the dark $\cdot\text{OH}$ generation.

This fact cannot be explained only by “direct” $\cdot\text{OH}$ generation via reaction (2) with the participation of thermalized h^+ formed at X-ray irradiation because as it was shown in Figure 3, the amount of hydroxyl radicals is increased with X-ray irradiation time, but by different UV light pre-treatment regimes.

(iv) We assume that one more mechanism is responsible for X-ray-induced $\cdot\text{OH}$ generation in L-GdYVO NPs. The presented data indicate that this mechanism appears to be associated with the h^+ formed in the NPs’ VB at UV light pre-treatment and trapped in local levels formed by RSP [39]. X-ray irradiation and an excess of energy released during h^+ thermalization can activate trapped holes and facilitate their jump movement towards the surface of NPs, increasing, consequently, the amount of generated $\cdot\text{OH}$. Note that the $\cdot\text{OH}$ generation by the mechanism associated with X-ray-facilitated h^+ jumps is more effective than direct $\cdot\text{OH}$ generation with the participation of thermalized h^+ because as seen in Figure 4a–c, column 2, in D-GdYVO NPs $\cdot\text{OH}$ scavenging is dominant even after 30 min (and longer) of X-ray exposure, and X-ray-induced $\cdot\text{OH}$ generation, which is expected to occur also in these NPs, does not become noticeable.

To separate the contribution of X-ray-facilitated h^+ jump effects, we have subtracted the amount of $\cdot\text{OH}$ generated as a result of water radiolysis in the solutions containing D-GdYVO (Figure 4a–c, column 2) from the total X-ray-induced $\cdot\text{OH}$ generation (Figure 4a–c, column 5). Thus, Figure 5 represents the contribution of all processes observed in aqueous solutions containing D-GdYVO and L-GdYVO NPs.

It is worth mentioning again that the total amount of OH generated in the aqueous solution containing L-GdYVO NPs at X-ray irradiation is much higher than that in the control solution representing X-ray-induced water radiolysis (Figure 4a–c, columns 1 and 3), which directly points to the potential of L-GdYVO NPs as NREs for RT.

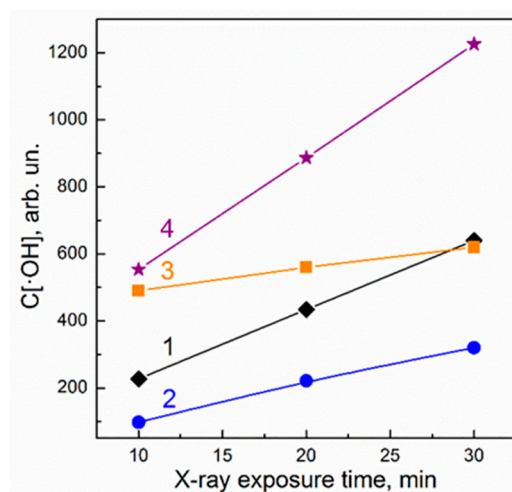


Figure 5. The contribution of different processes observed in the solution containing D-GdYVO and L-GdYVO at X-ray exposure: 1—control; 2—radioprotective effect (D-GdYVO); 3—OH dark generation (L-GdYVO); 4—X-ray-facilitated jumps of h^+ effect.

4. Conclusions

The obtained experimental data show that a preliminary treatment of GdYVO NPs with UV light is an effective tool allowing their redox properties to be changed drastically. GdYVO NPs that were UV light pre-treated (L-GdYVO) revealed strong $\cdot\text{OH}$ generation during further X-ray exposure, whereas GdYVO NPs, which were kept in the dark (D-GdYVO), showed radioprotective action. The mechanism of D-GdYVO radioprotective action ($\cdot\text{OH}$ scavenging) is ascribed to the presence of $\text{V}^{4+}-\text{V}_\text{O}-\text{V}^{4+}$ complexes in the crystal lattice of GdYVO. Electrons stored in vanadium ions participate in the neutralization of $\cdot\text{OH}$ formed at both water radiolysis and water splitting via reaction with the h^+ -mediated reaction.

The mechanism of X-ray-induced $\cdot\text{OH}$ generation in L-GdYVO is more complicated; two processes could be separated: (i) direct $\cdot\text{OH}$ generation with the participation of thermalized h^+ formed at X-ray irradiation, and (ii) X-ray-facilitated jumps of h^+ formed in the VB at UV light pre-treatment and trapped in local levels formed by RSP.

Thus, depending on the pre-treatment condition, we can change the redox properties of GdYVO in an opposite direction, which makes this nanomaterial a unique theranostic agent for RT enhancement, allowing the problem of RT-resistant hypoxic tumours to be overcome.

Author Contributions: Conceptualization, Y.V.M. and P.O.M.; Methodology, O.D.O. and K.O.H.; Investigation, P.O.M., K.O.H., S.L.Y., V.K.K., V.V.O.; Writing—original draft preparation, S.L.Y.; Writing—review and ending, Y.V.M., P.O.M., S.L.Y., K.O.H., V.V.O.; All authors have read and agreed to the published version of the manuscript.

Funding: This research was funded by National Academy of Sciences of Ukraine (Project no. 0119U100918).

Conflicts of Interest: The authors declare no conflict of interest.

References

- Delaney, G.; Jacob, S.; Featherstone, C.; Barton, M. The Role of Radiotherapy in Cancer Treatment. *Cancer* **2005**, *104*, 1129–1137. [[CrossRef](#)]
- Grubbé, E.H. Priority in the Therapeutic Use of X-rays. *Radiology* **1933**, *21*, 156–162. [[CrossRef](#)]
- Goel, S.; Ni, D.; Cai, W. Harnessing the Power of Nanotechnology for Enhanced Radiation Therapy. *ACS Nano* **2017**, *11*, 5233–5237. [[CrossRef](#)] [[PubMed](#)]
- Baskar, R.; Lee, K.A.; Yeo, R.; Yeoh, K.-W. Cancer and Radiation Therapy: Current Advances and Future Directions. *Int. J. Med. Sci.* **2012**, *9*, 193–199. [[CrossRef](#)] [[PubMed](#)]
- La Caer, S. Water radiolysis: Influence of oxide surfaces on H_2 Production under ionizing. *Radiat. Water* **2011**, *3*, 235–253. [[CrossRef](#)]

6. Buxton, G.V.; Mozumder, A.; Hatano, Y. The Radiation Chemistry of Liquid Water: Principles and Applications. In *Charged Particle and Photon Interactions with Matter*; Marcel Dekker: New York, NY, USA, 2004; Volume 4, pp. 331–363.
7. Kwatra, D.; Venugopal, A.; Anant, S. Nanoparticles in Radiation Therapy: A Summary of Various Approaches to Enhance Radiosensitization in Cancer. *Transl. Cancer Res.* **2016**, *2*, 330–342.
8. Haume, K.; Rosa, S.; Grellet, S.; Śmiałek, M.A.; Butterworth, K.T.; Solov'yov, A.V.; Prise, K.M.; Golding, J.; Mason, N.J. Gold nanoparticles for cancer radiotherapy: A review. *Cancer Nano* **2016**, *7*, 8–16. [[CrossRef](#)]
9. Wakefield, G.; Gardener, M.; Stock, M.; Adair, M. Nanoparticle Augmented Radiotherapy using Titanium Oxide Nanoparticles. *J. Nanomater. Mol. Nanotechnol.* **2018**, *7*, S6:002. [[CrossRef](#)]
10. Brunner, B.; Nestle, U.; Grosu, A.-L.; Partridge, M. SBRT in pancreatic cancer: What is the therapeutic window? *Radiother. Oncol.* **2014**, *114*, 109–116. [[CrossRef](#)]
11. Chen, X.; Song, J.; Chen, X.; Yang, H. X-ray-activated nanosystems for theranostic applications. *Chem. Soc. Rev.* **2019**, *48*, 3073–3101. [[CrossRef](#)]
12. Paro, A.D.; Shanmugam, I.; van de Ven, A.L. Nanoparticle-Mediated X-Ray Radiation Enhancement for Cancer Therapy. *Methods Mol. Biol.* **2017**, *1530*, 391–401.
13. Kuncic, Z.; Lacombe, S. Nanoparticle radio-enhancement: Principles, progress and application to cancer treatment. *Phys. Med. Biol.* **2018**, *63*, 02TR01. [[CrossRef](#)] [[PubMed](#)]
14. Kobayashi, K.; Usami, N.; Porcel, E.; Lacombe, S.; Le Sech, C. Enhancement of radiation effect by heavy elements. *Mutat. Res.* **2010**, *704*, 123–131. [[CrossRef](#)] [[PubMed](#)]
15. Her, S.; Jaffray, D.A.; Allen, C. Gold nanoparticles for applications in cancer radiotherapy: Mechanisms and recent advancements. *Adv. Drug Deliv. Rev.* **2015**, *109*, 84–101. [[CrossRef](#)]
16. Retif, P.; Pinel, S.; Toussaint, M.; Frochot, C.; Chouikrat, C.; Bastogne, T.; Barberi-Heyob, M. Nanoparticles for Radiation Therapy Enhancement: Key parameters. *Theranostics* **2015**, *5*, 1030–1044. [[CrossRef](#)]
17. Butterworth, K.T.; McMahon, S.J.; Currell, F.J.; Prise, K.M. Physical basis and biological mechanisms of gold nanoparticle radiosensitization. *Nanoscale* **2012**, *4*, 4830–4838. [[CrossRef](#)] [[PubMed](#)]
18. Marill, J.; Anesary, N.M.; Zhang, P.; Vivet, S.; Borghi, E. Hafnium Oxide Nanoparticles: Toward an in vitro predictive biological effect? *Radiat. Oncol.* **2014**, *9*, 150–161. [[CrossRef](#)] [[PubMed](#)]
19. Verry, C.; Sancey, L.; Dufort, S.; Le Duc, G.; Mendoza, C.; Lux, F.; Grand, S.; Arnaud, J.; Quesada, J.L.; Villa, J.; et al. Treatment of multiple brain metastases using gadolinium nanoparticles and radiotherapy: NANO-RAD, a phase I study protocol. *BMJ Open* **2019**, *9*, e023591. [[CrossRef](#)]
20. Lux, F.; Sancey, L.; Bianchi, A.; Cremillieux, Y.; Roux, S.; Tillement, O. Gadolinium-based nanoparticles for theranostic MRI-radiosensitization. *Nanomedicine* **2015**, *10*, 1801–1816. [[CrossRef](#)]
21. Sancey, L.; Lux, F.; Kot, S.; Roux, S.; Dufort, S.; Bianchi, A. The use of theranostic gadolinium-based nanoprobe to improve radiotherapy efficacy. *Br. J. Radiol.* **2014**, *87*, 20140134. [[CrossRef](#)]
22. Hainfeld, J.F.; Ridwan, S.M.; Stanishvskiy, Y.; Panchal, R.; Slatkin, D.N.; Smilowitz, H.M. Iodine nanoparticles enhance radiotherapy of intracerebral human glioma in mice and increase efficacy of chemotherapy. *Sci. Rep.* **2019**, *9*, 4505. [[CrossRef](#)] [[PubMed](#)]
23. Yefimova, S.L.; Maksimchuk, P.O.; Seminko, V.V.; Kavok, N.S.; Klochkov, V.K.; Hubenko, K.A.; Sorokin, A.V.; Kurilchenko, I.Y.; Malyukin, Y.V. Janus-Faced Redox Activity of LnVO₄:Eu³⁺ (Ln = Gd, Y, and La) Nanoparticles. *J. Phys. Chem. C* **2019**, *123*, 15323–15329. [[CrossRef](#)]
24. Grygorova, G.; Klochkov, V.; Mamotyuk, Y.; Malyukin, Y. Cerium Dioxide CeO_{2-x} and Orthovanadate (Gd_{0.9}Eu_{0.1}VO₄) Nanoparticles for Protection of Living Body from X-Ray Induced Damage. In *Nanomaterials for Security*; Bonca, J., Kruchinin, S., Eds.; Springer: Dordrecht, The Netherlands, 2016; pp. 289–296.
25. Maksimchuk, P.O.; Yefimova, S.L.; Hubenko, K.O.; Omeliaeva, V.V.; Kavok, N.S.; Klochkov, V.K.; Sorokin, A.V.; Malyukin, Y.V. Dark Reactive Oxygen Species (ROS) Generation in ReVO₄:Eu³⁺ (Re=Gd, Y) Nanoparticles in Aqueous Solutions. *J. Phys. Chem. C* **2020**, *124*, 3843–3850. [[CrossRef](#)]
26. Cooper, D.R.; Bekah, D.; Nadeau, J.L. Gold nanoparticles and their alternatives for radiation therapy enhancement. *Front. Chem.* **2014**, *2*, 86. [[CrossRef](#)]
27. Klochkov, V.K. The water solution of nanoluminophores nReVO₄:Eu³⁺ (Re = Y, Gd La). *Nanostruct. Materialoved.* **2009**, *2*, 3–8.
28. Ashawa, S.C.; Kini, U.R.; Madhvanath, U. The Aqueous Coumarin System as a Low Range Chemical Dosimeter. *Int. J. Appl. Radiat. Isot.* **1979**, *30*, 7–10. [[CrossRef](#)]

29. Xu, Z.H.; Li, C.X.; Hou, Z.Y.; Pang, C.; Lin, J. Morphological Control and Luminescence Properties of Lanthanide Orthovanadate LnVO₄ (Ln= La to Lu) Nano-/microcrystals via Hydrothermal Process. *CrystEngComm* **2011**, *13*, 474–482. [[CrossRef](#)]
30. Yang, P.; Huang, S.; Kong, D.; Lin, J.; Fu, H. Luminescence Functionalization of SBA-15 by YVO₄: Eu³⁺ as a Novel Drug Delivery System. *Inorg. Chem.* **2007**, *46*, 3203–3211. [[CrossRef](#)]
31. Su, Y.; Li, G.; Xue, Y.; Li, L. Tunable physical properties of CaWO₄ nanocrystals via particle size control. *J. Phys. Chem. C* **2007**, *111*, 6684–6689. [[CrossRef](#)]
32. Nakamoto, K. *Infrared and Raman Spectra of Inorganic and Coordination Compounds*, 6th ed.; John Wiley & Sons: Hoboken, NJ, USA, 2009; p. 432.
33. Hsu, C.; Powell, R.C. Energy transfer in Europium doped Yttrium Vanadate crystals. *J. Lumin.* **1975**, *10*, 273–293. [[CrossRef](#)]
34. Ronde, H.; Blasse, G. The nature of the electronic transitions of the vanadate group. *J. Inorg. Nucl. Chem.* **1978**, *40*, 215–219. [[CrossRef](#)]
35. Yang, L.; Li, G.; Hu, W.; Zhao, M.; Sun, L.; Zheng, J.; Yan, T.; Li, L. Control Over the Crystallinity and Defect Chemistry of YVO₄ Nanocrystals for Optimum Photocatalytic Property. *Eur. J. Inorg. Chem.* **2011**, *14*, 2211–2220. [[CrossRef](#)]
36. Takeshita, S.; Watanabe, T.; Isobe, T.; Sawayama, T.; Niikura, S. Improvement of the photostability for YVO₄:Bi³⁺,Eu³⁺ nanoparticles synthesized by the citrate route. *Opt. Mater.* **2011**, *33*, 323–326. [[CrossRef](#)]
37. Takeshita, S.; Ogata, H.; Isobe, T.; Sawayama, T.; Niikura, S. Effects of Citrate Additive on Transparency and Photostability Properties of YVO₄:Bi³⁺, Eu³⁺ Nanophosphor. *J. Electrochem. Soc.* **2010**, *157*, 74–80. [[CrossRef](#)]
38. Garces, N.Y.; Stevens, K.T.; Foundos, G.K.; Halliburton, L.E. Electron paramagnetic resonance and optical absorption study of V⁴⁺ centers in YVO₄ crystals. *J. Phys. Condens. Matter.* **2004**, *16*, 7095–7106. [[CrossRef](#)]
39. Lifshitz, I.M. The energy spectrum of disordered systems. *Adv. Phys.* **1964**, *13*, 483–536. [[CrossRef](#)]
40. Yefimova, S.L.; Maksimchuk, P.O.; Hubenko, K.A.; Klochkov, V.K.; Borovoy, I.A.; Sorokin, A.V.; Malyukin, Y.V. Untangling the Mechanisms of GdYVO₄:Eu³⁺ Nanoparticle Photocatalytic Activity. *Colloid Surf. A* **2019**, *577*, 630–636. [[CrossRef](#)]



© 2020 by the authors. Licensee MDPI, Basel, Switzerland. This article is an open access article distributed under the terms and conditions of the Creative Commons Attribution (CC BY) license (<http://creativecommons.org/licenses/by/4.0/>).